Journal of Alloys and Compounds 904 (2022) 164016

Contents lists available at ScienceDirect

Journal of Alloys and Compounds

journal homepage: www.elsevier.com/locate/jalcom

Promising Tb^{3+}-doped gallium tungsten-phosphate glass scintillator: Spectroscopy, energy transfer and UV/X-ray sensing

Thiago A. Lodi[a,*], Jéssica F.M. dos Santos[a,*], Gustavo Galleani[a], Luiz G. Jacobsohn[b], Tomaz Catunda[a], Andrea S.S. de Camargo[a,*]

[a] São Carlos Institute of Physics, University of São Paulo, Av. Trabalhador Saocarlense 400, São Carlos, SP, 13566-590, Brazil
[b] Department of Materials Science and Engineering, Clemson University, 515 Calhoun Dr, Clemson, SC, 29634, USA

ARTICLE INFO

Article history:
Received 28 December 2021
Received in revised form 22 January 2022
Accepted 27 January 2022
Available online 31 January 2022

Keywords:
Scintillators
Gallium tungsten phosphate glasses
Terbium
Energy transfer

ABSTRACT

Undoped and Tb^{3+}-doped (0.5–10 mol%) gallium tungsten-phosphate glasses, in the new compositional system $NaPO_3$-Ga_2O_3-Na_2WO_4, were prepared and characterized by UV–visible absorption, photoluminescence excitation and emission, excited state decay measurements and X-ray excited radioluminescence measurements. A detailed study of ion-ion energy transfer, based on the analysis of decay curves by the Inokuti-Hirayama model, indicated that the energy transfer process affecting the emitting level $^5D_3$ of Tb^{3+} is related to dipole–dipole interaction. Additionally, a theoretical model was successfully employed to establish a correlation between the emission color variation due to changes in the green to blue emission ratio (I_G/I_B). The emission spectra of the undoped and Tb^{3+}-doped glasses were measured under UV and X-ray excitation. From the viewpoint of UV-sensing, samples doped with up to 7.0 mol% Tb^{3+} do not present visible emission quenching, whereas X-ray sensing is not prone to quenching at all up to 10 mol% Tb^{3+} doping. These characteristics, associated to a relatively high density, highlight the potential of these glasses as X-ray scintillators.

1. Introduction

A scintillator functions as a wavelength shifter. It converts the energy of a charged particle (α and β, for example) or high energy photons, such as UV, X-rays and γ-ray, into several low energy photons in the visible or near-visible range of the electromagnetic spectrum. These photons, in turn, can be more easily detected by photodetectors such as photodiodes (PD) and photomultiplier tubes (PMTs) [1], enabling scintillators for diverse applications such as in industrial and medical imaging, homeland security and high energy physics experiments [2,3]. The luminescence centers in scintillators can be intrinsic or extrinsic in nature. Intrinsic luminescence mainly involves ions or chemical groups composing the scintillator. Extrinsic luminescence, on the other hand, originates from metallic dopant ions, commonly involving the *f-f* and *f-d* transitions of Tb^{3+}, Eu^{2+} and Ce^{3+} [1,4,5]. Typically, scintillators are made from inorganic single crystals with high emission efficiency and energy resolution, such as $LaBr_3$:Ce and BGO that are commercially available scintillators [6]. However, the growth of single-crystals is time-consuming, expensive, and results in materials with limited sizes and shapes. For this reason, increasing interest has been demonstrated for glass scintillators, which can provide cost-effective, large-scale production, being easily processed into complex geometries, including optical fibers [7].

Despite the fact that many compositions have been explored for optical applications, phosphate glasses remain, perhaps, the most interesting materials on account of their top-notch physical properties such as high thermal expansion coefficient and easy processing due to the low melting temperature (compared to silicate glasses) [8–11]. Besides, phosphate glasses allow for higher rare earth (RE) ions solubility than other oxide glassy matrices such as silicates and borates, i.e., the RE luminescence quenching usually occurs at very high (> 5 mol%) RE doping concentration. However, these glasses have relatively poor chemical stability, which often limits their applications. In this context, considerable work has been carried out on improving the physical-chemical properties of phosphate glasses by introducing several glass formers and modifiers such as CaO, MoO_3, Ga_2O_3, WO_3, Ta_2O_3, Sb_2O_3, etc., [12–15]. Through the proper choice of these metal oxides, the structural network of phosphate -based glasses can be modified to increase their chemical, thermal and mechanical stability, their luminescence characteristics,

* Corresponding authors.
E-mail addresses: augustolodi@usp.br (T.A. Lodi), jessica.santos@usp.br (J.F.M. dos Santos), andreasc@ifsc.usp.br (A.S.S. de Camargo).

https://doi.org/10.1016/j.jallcom.2022.164016
0925-8388/

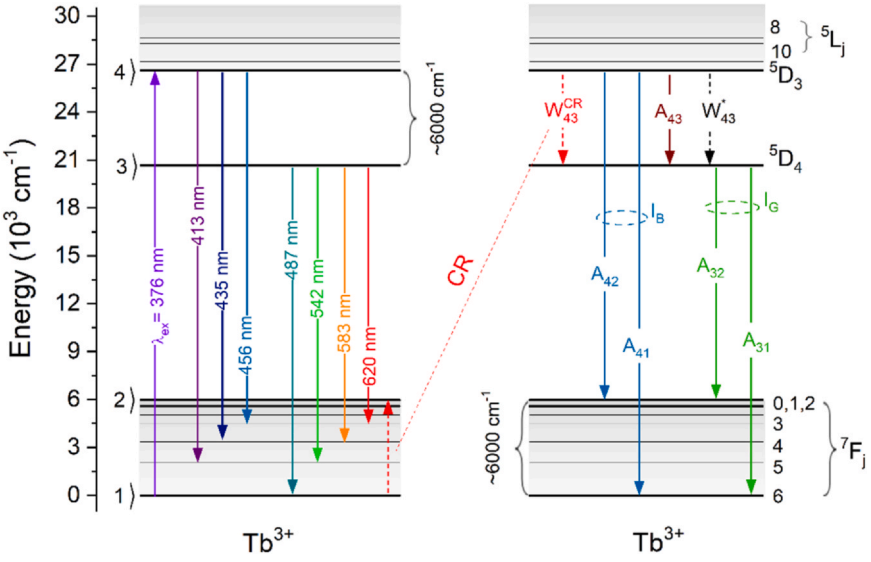

Fig. 1. Partial energy level diagram of Tb^{3+} illustrating the excitation power rate (R_{14}), radiative decay rates (A_{31}, A_{32}, A_{41}, A_{42}, A_{43}), the cross-relaxation process (W_{43}^{CR}) and W_{43}^{*} which corresponds to the sum of all decay rates from $^5D_3$.

biocompatibility, etc. The new glass system investigated in this work is based on the composition $NaPO_3$-Ga_2O_3-Na_2WO_4 (NaPGaW). The addition of both Na_2WO_4 [14,16] and Ga_2O_3 [17,18] modifiers is known to enhance mechanical, and thermal stabilities, chemical durability of phosphate glasses and makes this glass system interesting for optical applications. Moreover, the incorporation of tungsten is responsible for increasing the glass density and possibly for decreasing the phonon energy of the phosphate network. The increase of the glass density can also enhance the probability of interaction of the ionizing radiation with matter, an essential feature for scintillators [19].

Among the RE ions that present 4–4f transitions, known to have strong emission in the UV–visible-IR region, Tb^{3+} is one of the most interesting dopants with potential for application in solid state lasers, scintillators, biological detectors, white light generators, field emission and other fluorescent devices [20–22]. The characteristic emissions of this ion originating from the metastable levels $^5D_3$ (379–456 nm) and $^5D_4$ (487–620 nm), are susceptible to the presence of energy transfer (ET) mainly through the cross-relaxation mechanism (W_{43}^{CR}, in Fig. 1). In this process, electronic population is transferred from the level $^5D_3$ to $^5D_4$ [21–23], imposing a quenching to the emission from the donor level $^5D_3$ and favoring the emission from $^5D_4$.

Typical host media (insulators or wide bandgap semiconductors) exert limited influence on the RE transitions due to the effective screening of 4 f electrons by the outer shell orbitals 5p, 5d and 6s. Since the first terbium-activated glass was reported [24], numerous glass compositions have been proposed, such as barium silicate[25], tungsten gadolinium borate [26] and borogermanate glasses [27]. However, to the best of our knowledge, Tb^{3+}-doped gallium tungsten-phosphate glass scintillators have not been investigated. The high Tb concentration limit prior to quenching, associated to long radiative lifetime values (ms) and the green emission which matches commercial photodetectors, such as charge coupled device (CCD) and silicon PMT, allow detection of high-energy excitation radiation. [28].

In this work, we present detailed spectroscopic investigation of these novel NaPGaW glasses with special emphasis on the energy transfers involving Tb^{3+} ions. Because the excited states $^5D_3$ and $^5D_4$ are connected via a cross relaxation mechanism, whose efficiency depends on Tb^{3+} concentration, a thorough characterization is important to determine the optimum range of dopant concentration for the intended application as a scintillator glass. The fluorescence decay curves, which carry the excited state dynamics information, were fit using the Inokuti-Hirayama (IH) model, while the color of the samples, associated to the ratio of green to blue emission intensity I_G/I_B was modeled and correlated to the quantum efficiencies. Last but not least, the characterization of the doped glasses intense emission spectra upon UV and X-ray excitation is presented, which, associated to the excellent mechanical and chemical stability, and high density of the glasses indicates their promising use as scintillators.

2. Experimental procedure

Undoped and Tb^{3+} doped gallium tungsten-phosphate glasses with composition $60NaPO_3$–$(20\text{-}x)Ga_2O_3$–$20Na_2WO_4.2H_2O$–$xTbCl_3.6H_2O$ (x = 0, 0.5, 1, 3, 5, 7 and 10 mol%) were obtained by the melt-quenching technique. Stoichiometric batches of the solid starting materials (≥ 99,9% purity) were mixed in an agate mortar and melted in a platinum crucible, in an electric furnace at 1000–1100ºC, for 1 h, in air atmosphere. Immediately after the quenching, the melt was poured into a preheated stainless-steel mold at 280 ºC. In order to minimize the internal mechanical stress, the glasses were annealed at 300 °C for 4 h and then slowly cooled to ambient temperature. Finally, the glasses were cut and optically polished with 2 mm thickness. The nominal compositions and respective sample labeling are given in Table 1 along with the values of volumetric density (ρ). The density values were calculated according to the Archimedes principle, using distilled water as an immersion liquid, at room temperature.

Table 1
Glass label, nominal composition (mol%) and volumetric density (ρ).

Glass label	Nominal composition (mol%)				ρ (g.cm^{-3})
	$NaPO_3$	Ga_2O_3	Na_2WO_4	$TbCl_3$	
NaPGa	80	20	–	–	3.04
NaPGaW20	60	20	20	0	3.62
NaPGaW0.5Tb	60	19.5	20	0.5	3.63
NaPGaW1Tb	60	19	20	1	3.63
NaPGaW3Tb	60	17	20	3	3.60
NaPGaW5Tb	60	15	20	5	3.72
NaPGaW7Tb	60	13	20	7	3.70
NaPGaW10Tb	60	10	20	10	3.82

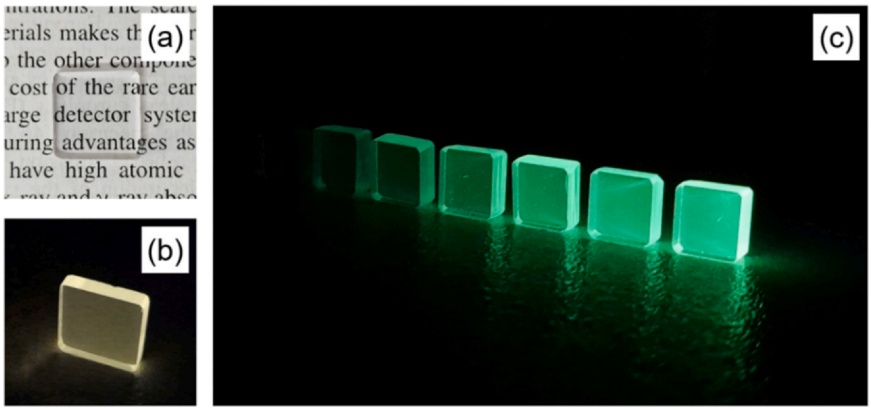

Fig. 2. Photographs of the undoped glass under (a) ambient light, and (b) UV excitation (326 nm). (c) Photographs of the Tb^{3+} doped glasses under UV lamp excitation (376 nm), in ascending order of Tb-concentration (0.5, 1.0, 3.0, 5.0, 7.0 and 10.0 mol%) from left to right.

The UV–visible-NIR ground state absorption spectra of the samples were recorded using a Perkin-Elmer Lambda 1050 double-beam spectrometer in the range 250–800 nm with a spectral resolution of 1 nm. Photoluminescence (PL) excitation and emission spectra of the undoped and Tb^{3+}-doped glasses were recorded with a HORIBA Jobin Yvon spectrofluorometer model Fluorolog-3, equipped with 450 W CW Xenon arc lamp as an excitation source. The excited state lifetime values were measured in the same equipment, using a pulsed Xe lamp. Radioluminescence (RL) measurements were recorded with a Freiberg Instruments Lexsyg Research spectrofluorometer equipped with a Varian Medical Systems VF-50J X-ray tube with a tungsten target operated at 40 kV and 1 mA, and an Andor Technology Shamrock 163 spectrograph coupled to an Andor Technology DU920P-BU Newton CCD camera kept at − 80 °C.

3. Results and discussion

All the glass samples were obtained colorless and transparent with good chemical stability under ambient conditions. Photographs of the undoped NaPGaW and NaPGaW:Tb^{3+} samples under ambient light and UV lamp excitation are shown in Fig. 2.

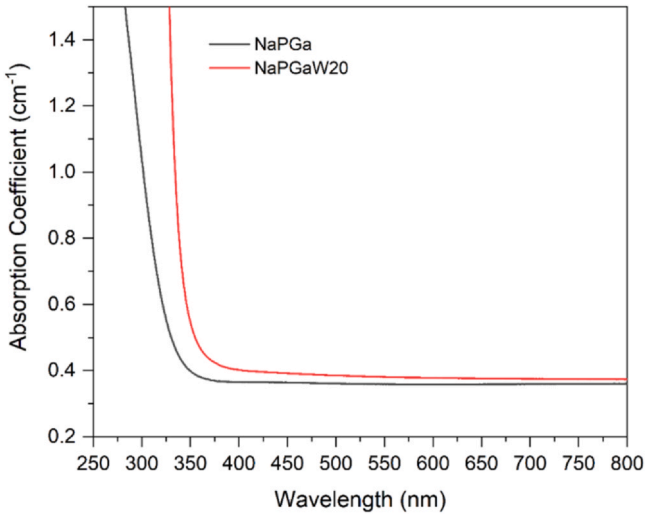

Fig. 3. Ground state absorption spectra of NaPGa and NaPGaW20 glasses in the UV–visible region.

3.1. Undoped glasses

According to Table 1, the undoped NaGaW20 glass presented higher density than the analog glass NaPGa without sodium tungstate. This result is expected due to the higher molar density of $Na_2WO_4.2\,H_2O$ ($\rho \sim 4.18\,g.cm^{-3}$) when compared to that of $NaPO_3$ ($\rho \sim 2.48\,g.cm^{-3}$). The volumetric density value of the NaPGaW20 glass is similar to that of the commercially available inorganic single crystal scintillator NaI:Tl ($3.67\,g.cm^{-3}$) [29] and superior to the value for the ^{6}Li-glass scintillator (Ce^{3+}-doped ^{6}Li silicate, GS20®) ($2.5\,g.cm^{-3}$) [30].

Fig. 3 presents the absorption spectra of the NaPGa and NaPGaW20 samples, recorded in the wavelength range 250–800 nm. A wide transmittance window indicates that both glasses are suitable for rare earth ion doping. It can also be seen that when adding Na_2WO_4, the absorption edge of the NaPGaW20 glass in the UV shifts towards longer wavelengths (redshifts) when compared to the NaPGa glass. This behavior can be explained by the increase of the covalent character of the vitreous network, attributed to the insertion of WO_n polyhedra. The latter link PO_4 groups forming a highly covalent three-dimensional network [31,32].

It is well known that tungsten cations present four oxidation states from W^{3+} to W^{6+}, and the amount of each oxidation state is dependent on the composition and melting conditions of the glass. It is, therefore, important to determine such oxidation states in the glasses. The strong UV absorption band around 350 nm due to the charge transfer of hexavalent tungsten state (W^{6+}), and the absence of an absorption band at ~780 nm, as well as of blueish color in the glasses, indicates the existence of mainly hexavalent oxidation state in these glasses [16].

Fig. 4 shows the PL excitation and emission spectra of the NaPGaW20 glass and the PL emission spectra of the NaPGa glass for comparison. In the case of NaPGaW20, a wide emission band centered at approximately 570 nm, corresponding to the yellow emission seen in Fig. 2(b), can be observed. Scheike et al. [33] reported an emission centered at $\lambda = 530$ nm in WO_3-P_2O_5-ZnO glass. Wen et al. [34], observed a similar emission band centered at 465 and 496 nm in the tungsten-doped glasses $(Na_2WO_4.2\,H_2O)_{0.01}(PbO)_{49.99}(B_2O_3)_{50}$ and $(Na_2WO_4.2\,H_2O)_{0.5}(PbO)_{49.5}(B_2O_3)_{50}$, upon excitation at 332 and 343 nm, respectively. The $(WO_3)_{0.5}(SiO_2)_{49.5}(Na_2O)_{25}(B_2O_3)_{25}$ glass showed a broader and stronger emission band at 520 nm under excitation at 300 nm [34]. In crystals, such as $ZnWO_4$, $CdWO_4$ and $MgWO_4$, the broad band at approximately 540 nm is ascribed to the radiative decay of self-trapped excitons (STEs) at the (WO_6^{6-}) complex [35]. Based on these observations, the emission at about 570 nm was ascribed to the (WO_6^{6-}) ion.

In the last years, attempts have been made to explain the STE radiative decay such as the model proposed by Korzhik et al. [36] and the model proposed by Leonelli and Brebner [37]. While differing in many aspects, one point is consensus: Luminescence seems to be associated with defects promoted by distortions in the structure.

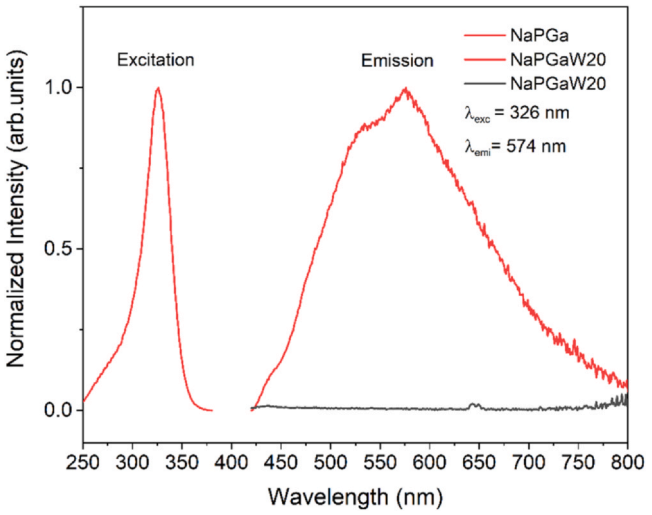

Fig. 4. Photoluminescence excitation and emission spectra of NaPGa (black spectrum) and NaPGaW20 (red spectra) glasses.

Recently, a new model known as broad band model was proposed. This model assumes that there are energetically distributed states related to point defects such as oxygen vacancies. These states, located above the valence band and below the conduction band, can promote the captured electrons to the conduction band by photons absorption, creating small polarons. This polarons interact with holes trapped in the crystal defects or impurities forming STEs that are responsible for the emission in the visible range [38,39].

The excitation spectrum of the NaPGaW20 glass monitored at 576 nm shows a broad excitation band peaked around 326 nm. In $ZnWO_4$ crystals [40] and other forms [41], this excitation band is assigned to charge-transfer transitions from the oxygen (O^{2-}) to the tungsten (W^{6+}) ions in the WO_6 molecular complexes.

Besides UV excitation, the emission spectra of the undoped gallium tungsten-phosphate glasses were also investigated under X-ray excitation. The room temperature RL spectra shown as Fig. 5 presents a broadband emission band centered at 540 nm, very similar to the band observed upon UV excitation, and which was attributed to the radiative decay of STEs at WO_6^{6-} complexes. Also, similar to the case of UV excitation, the NaPGa glass did not present any luminescence in the investigated range. It is worth noticing that this broad emission band observed under both, UV and X-ray excitation, overlaps quite well with the absorption range of CCD detectors and silicon photomultipliers [29], allowing for the use of these glasses as optical sensors.

3.2. Tb^{3+} doped samples

As it can be seen in Table 1, the volumetric density values of doped glasses increased with the increasing substitution of Ga_2O_3 by $TbCl_3.6\,H_2O$. As well as in the NaPGaW20 glass, the volumetric density of the Tb^{3+} gallium tungsten-phosphate glasses is similar to that of the commercially available inorganic single crystal scintillator NaI:Tl (3.67 g.cm^{-3}) [29], and superior to Tb silicate glass (3.03 g.cm^{-3}) [42] and ^{6}Li-glass scintillator (Ce^{3+}-doped ^{6}Li silicate, GS20®) (2.5 g.cm^{-3}) [30].

Fig. 1 shows the partial energy level diagram of Tb^{3+} in the energy scale up to 30×10^3 cm^{-1} above the ground state multiplet $^7F_6$ of the $4f^8$ configuration. Selected radiative transitions are indicated by continuous lines whereas non-radiative relaxation processes are indicated by dashed and curved lines. The rich energy level diagram favors detrimental intra- and interionic energy transfer processes. In particular, the resonant CR efficiently depopulates the emitting level $^5D_3$ at high doping levels [21,43,44], as it will be discussed throughout this section.

UV–visible-NIR absorption spectra of the NaPGaW:Tb^{3+} glasses are shown in Fig. 6. The strong absorption in the 320–400 nm range is associated with the onset of the WO_3 absorption band. In the UV–visible region, four absorption bands at 351 nm, 368 nm, 377 nm and 485 nm are assigned to the optical transitions of Tb^{3+} ($^7F_6 \rightarrow {}^5L_9$, $^5L_{10}$, $^5D_3$ and $^5D_4$), respectively. In the NIR region (inset), two absorption bands can be observed centered around 1900 nm and 2218 nm, assigned to the transitions $^7F_6 \rightarrow {}^7F_{0,1,2,3}$. Furthermore, it was found that all the absorption bands intensities increased with increasing $TbCl_3$ concentration.

Fig. 7(a) shows the excitation spectrum of the NaPGaW:5.0Tb glass measured by monitoring the green emission of Tb^{3+} ions at 542 nm. The excitation spectrum (black line) can be divided in two regions. One is a broadband predominant at wavelengths lower than 330 nm attributed to tungsten transitions. The other is composed of several peaks at 302, 316, 338, 350, 357, 367, 376 and 484 nm which correspond to the excitation transitions from the ground state ($^7F_6$) of Tb^{3+} to the excited states $^5H_6$, $^5H_7$, $^5L_7$, ($^5G_4$ + $^5L_9$), $^5G_5$, $^5L_{10}$, $^5D_3$ and $^5D_4$, respectively. The other Tb^{3+}-doped NaPGaW glasses showed identical excitation peaks position as the NaPGaW:5Tb glass sample. The linear dependence of the integrated area of $^7F_6 \rightarrow {}^5D_3$ (blue) and $^7F_6 \rightarrow {}^5D_4$ (green) absorption bands on the dopant concentration is

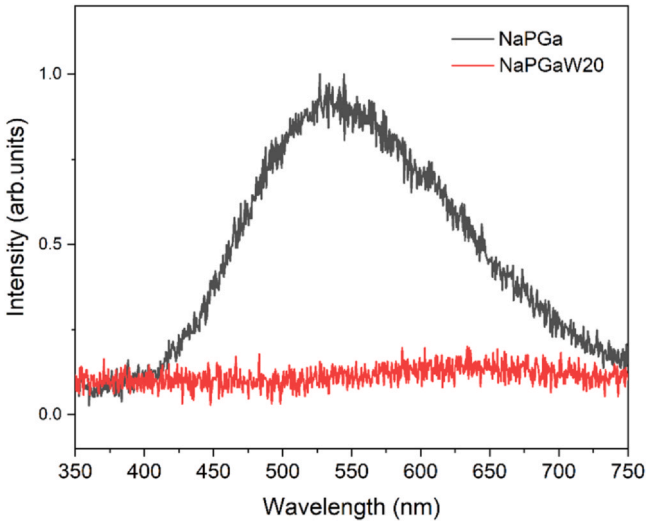

Fig. 5. Radioluminescence spectra of NaPGa and NaPGaW20 glasses under X-ray excitation.

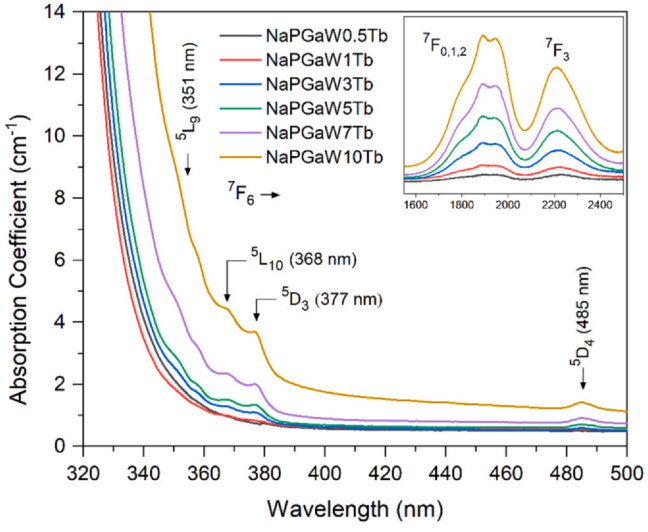

Fig. 6. Absorption spectra of NaPGaW:Tb^{3+} glasses in the UV–visible and IR region (inset).

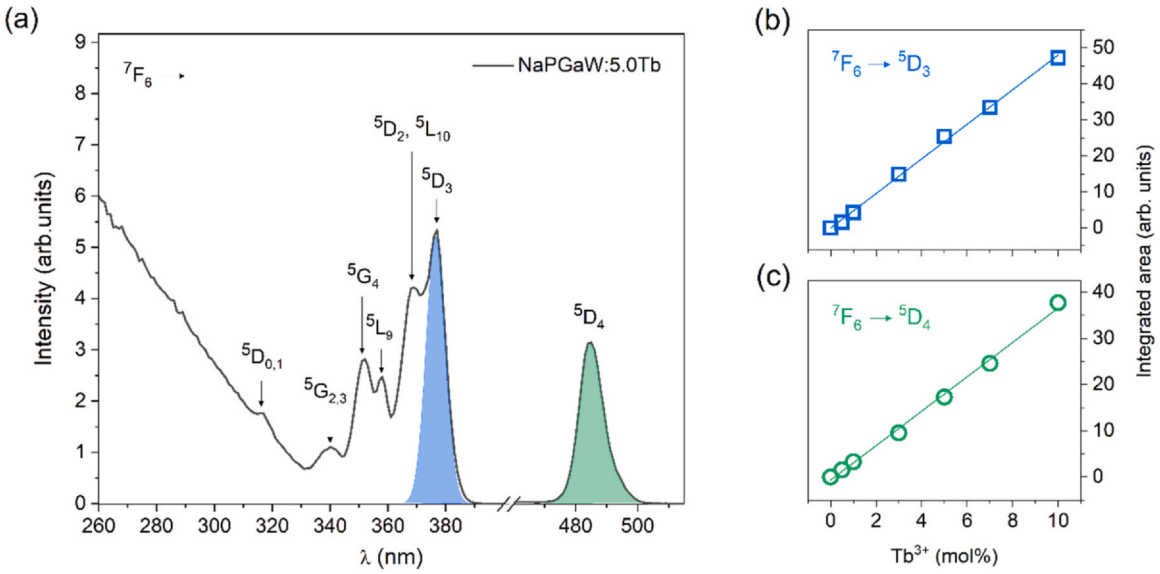

Fig. 7. (a) Excitation spectrum of NaPGaW:5.0Tb glass, λ_{em} = 542 nm. (b)-(c) The dependence of the $^5D_3$ and $^5D_4$ absorption bands (integrated area) on Tb^{3+} concentration.

shown in Fig. 7(b) and (c), respectively. The $^5D_3$ and $^5D_4$ levels are particularly important, since they are the only metastable levels of Tb^{3+} in the visible range.

The emission spectra of the NaPGaW:Tb^{3+}glasses were measured with excitation at 376 nm ($^7F_6 \rightarrow {}^5D_3$ transition, Fig. 1) and are shown in Fig. 8. In order to highlight the ET process and the luminescence behavior, each spectrum in Fig. 8 was normalized to the intensity of its highest peak ($^5D_4 \rightarrow {}^7F_5$). The peaks in the blue spectral region, I_B, (413, 435, 456 nm) are assigned to the $^5D_3 \rightarrow {}^7F_J$ (J = 5, 4, 3) transitions. The peaks in the green-red region, I_G, (487, 542, 583 and 620 nm) are assigned to $^5D_4 \rightarrow {}^7F_J$ (J = 6, 5, 4, 3) transitions. Among these transitions, the magnetic dipole one, corresponding to the green emission $^5D_4 \rightarrow {}^7F_5$ at 542 nm, is the most intense one, satisfying the selection rule $\Delta J = \pm 1$. All the emissions involving the $^5D_3$ state are markedly affected by the Tb^{3+} ion concentration. The blue to green color change of the fluorescence (see inset in Fig. 8) of the fluorescence is mainly due to the following CR mechanism [45–47]:

$$^5D_3 + {}^7F_0 \rightarrow {}^5D_4 + {}^7F_6, \quad (1)$$

since the energy gaps between $^5D_3$ - $^5D_4$ and $^7F_6$ - $^7F_0$ are remarkably similar (Fig. 1).

As discussed above, the glasses present variations of the relative emissions intensities depending on the doping content. The CIE 1931 coordinates of the Tb^{3+}-doped NaPGaW glasses were computed, as

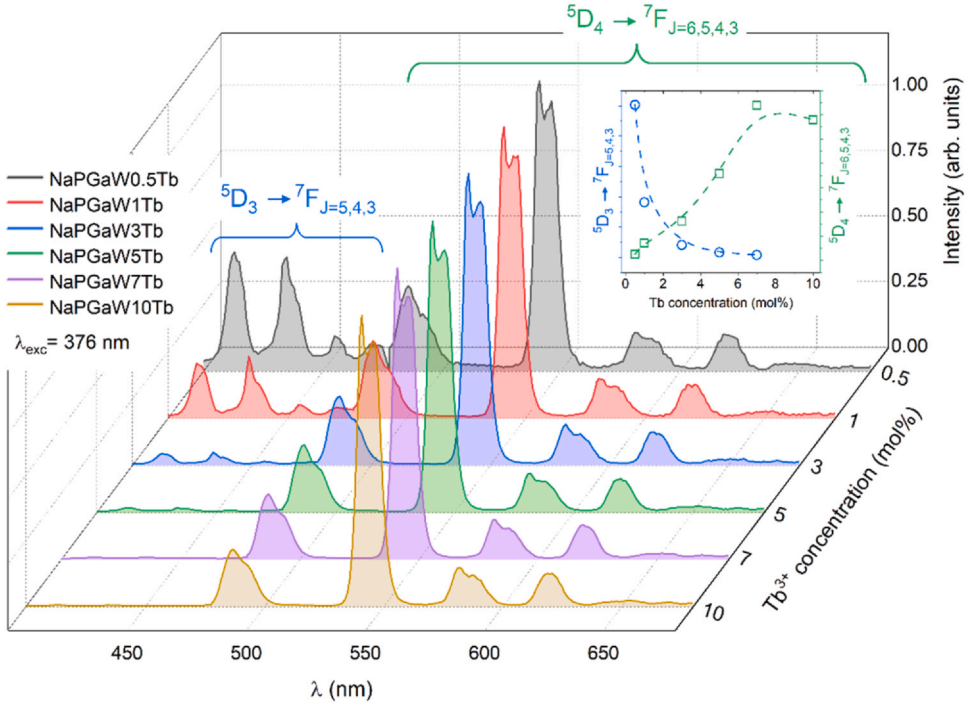

Fig. 8. Concentration dependence of the $^5D_3 \rightarrow {}^7F_J$ = 5–3 (blue) and $^5D_4 \rightarrow {}^7F_J$ = 6–3 (green) emission spectra under UV excitation (λ_{exc}= 376 nm) of Tb^{3+}- doped NaPGaW glasses. Each spectrum was normalized to the peak intensity of the $^5D_4 \rightarrow {}^7F_5$ transition (542 nm). Inset: Non-normalized integrated area of $^5D_3 \rightarrow {}^7F_j$ = 5–3 (blue circles) and $^5D_4 \rightarrow {}^7F_j$ = 6–3 (green squares) transitions as a function of Tb^{3+} concentration.

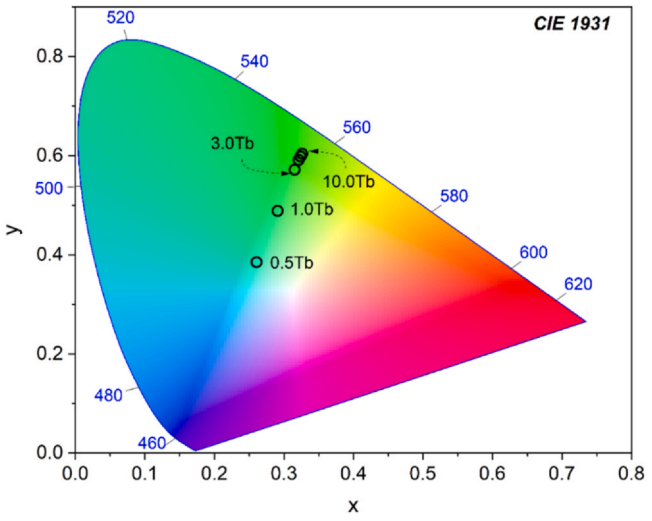

Fig. 9. CIE 1931 chromaticity diagram for Tb^{3+}-doped NaPGaW glasses under UV (376 nm) excitation.

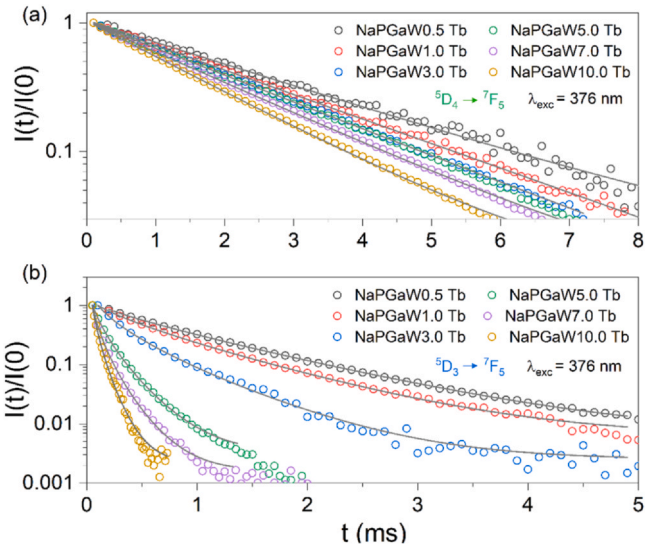

Fig. 10. Decay curves of (a) the $^5D_4 \rightarrow {}^7F_4$ emission and (b) the $^5D_3 \rightarrow {}^7F_4$ emission of Tb^{3+}-doped NaPGaW glasses. Solid gray lines are given by Eq. (3).

illustrated in Fig. 9 and Table 2. With a change in the Tb^{3+} ion concentration in the range of 0.5–10 mol%, the color coordinates of the samples were tuned from (0.2606, 0.38533) to (0.3261, 0.6042), namely, multicolor emissions could be achieved. Notably, the emitting-color of the samples gradually changes from blue to green, with an increase in the Tb^{3+} ion content. The CIE chromaticity coordinate of NaPGaW7.0Tb is close to commercial fluorescent powder $MgAl_{11}O_{19}$:0.67Ce^{3+},0.33Tb^{3+} (0.3300, 0.5950), suggesting that NaPGaWTb can also be a potential candidate in the solid white light field.

Fluorescence decay analysis is very helpful to understand the ET mechanisms and quenching behavior of Tb^{3+}-luminescence. Indeed, the fluorescence decay is determined by the addition of the radiative decay rate (A) to nonradiative processes due to ET processes (self-quenching, multiphonon emission (W^{MP}), hydroxyl groups (OH^-) and other impurities)[48]. Thus, the measured lifetime (τ^{exp}) can be expressed as follows

$$\frac{1}{\tau^{exp}} = A + W^{ET} + W^{MP} + W^{OH} + \ldots\ldots \quad (2)$$

Experimental emission $^5D_4$ and $^5D_3$ decay under UV (376 nm) excitation are presented in Fig. 10(a) and (b), respectively. The effective lifetimes were obtained from the fluorescent decay curves, I (t), by:

$$\tau^{exp} = \frac{\int_0^\infty t \quad I(t) \quad dt}{\int_0^\infty \quad I(t) \quad dt} \quad (3)$$

The $^5D_4 \rightarrow {}^7F_5$ emission decay curves presented in Fig. 10(a), were well fit by a single exponential function for all doping concentrations up to 10 mol%. However, the lifetime values decrease from 2.59 to 1.61 ms when Tb^{3+} concentration increases from 0.5–10 mol%. Such a behavior of the $^5D_4$ excited state lifetime is due to the large population of this level, which increases the probability of energy migration. As a minor effect, it could also directly lead to losses, e.g., energy transfer to some other undesired impurity or defect. However, the concentration dependence is weak, similarly to what was reported for Tb^{3+}-doped zinc phosphate [46] and fluoroborate [43] glasses. W^{MP} should be negligible due to the very large energy gap (~15000 cm^{-1}) below the $^5D_4$ level, corresponding to ~ 16-phonons considering the phonon cut-off frequency of the NaPGaW20 glass (~950 cm^{-1}). Therefore, we can conclude that the experimentally observed lifetime in the Tb^{3+} zero-concentration limit (τ_{30}^{exp}) should be close to $^5D_4$ radiative lifetime, $\tau_3^{rad} \sim \tau_{30}^{exp}$ = (2.59 ± 0.05) ms. Consequently, the concentration dependence of the $^5D_4$ quantum efficiency can be estimated by $\eta_3 = \tau_3^{exp}/\tau_{30}^{exp}$, as shown in Table 2.

The decay curves from the $^5D_3$ (level 4 in Fig. 1), on the other hand, exhibit a clear non-exponential character, as shown in Fig. 10(b). Their effective lifetimes, τ_4^{exp}, decrease from 0.82 to 0.07 ms, upon increasing the Tb^{3+} concentration from 0.5 m to 10 mol%. A similar behavior was observed in most Tb^{3+} doped materials (crystal and glasses) and attributed to the CR process given by Eq.(1) depicted in Fig. 1.

The decay curves can also provide some insight about the energy transfer microscopic parameters using the Inokuti–Hirayama (IH) model that assumes Tb^{3+} ions are randomly distributed in the glass structure [46,49–51]. For instance, considering $^5D_3$ - $^5D_4$ cross relaxation, it is possible to obtain the critical distance R_0 from the concentration quenching data. R_0 is defined as the critical separation

Table 2
Tb population density (N_t), concentration dependence of the blue-to-green intensity ratio under 376 nm excitation (I_G/I_B), the CIE chromaticity coordinates (x,y), the decay times τ_3^{exp} ($^5D_4$), τ_4^{exp} ($^5D_3$) and the $^5D_4$ fluorescence quantum efficiency, η_3.

Tb^{3+} (mol)	Tb^{3+} (× 10^{19} cm^{-3})	I_G/I_B	CIE (x,y)	τ_3^{exp} (± 0.04) ms	τ_4^{exp} (± 0.03) ms	η_3 (± 0.09)
0.5	2.90	2.1	0.2606, 0.3853	2.59	0.82	1.0
1.0	5.80	5.0	0.2909, 0.4890	2.27	0.62	0.88
3.0	17.4	22.1	0.3152, 0.5722	2.07	0.31	0.80
5.0	29.8	54.5	0.3211, 0.5916	2.03	0.17	0.78
7.0	41.8	112	0.3238, 0.5987	1.84	0.11	0.71
10.0	61.3	[a]	0.3261, 0.6042	1.61	0.066	0.62

[a] The I_G/I_B ratio was not calculated because $I_B \rightarrow 0$.

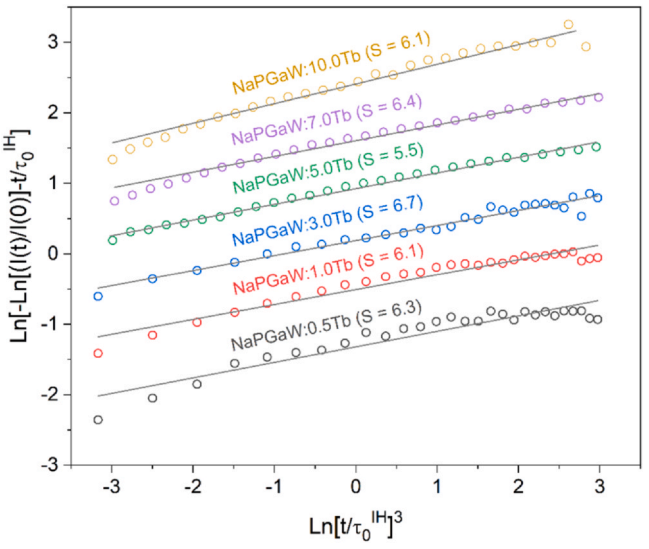

Fig. 11. Plots of experimental data $ln\left[-ln\left(\frac{I(t)}{I_0}\right)-\frac{t}{\tau_0^{IH}}\right]$ $versus ln\left(\frac{t}{\tau_0^{IH}}\right)^3$ relative to the blue emission. Solid gray lines best fits obtained using the Inokuti–Hirayama (IH) model (Eq.(4)).

between donor and acceptor at which the non-radiative rate equals to the radiative rate of the internal single-ion relaxation. According to IH model, fluorescence decay is given by [49].

$$I(t) = I_0 \exp\left[-\frac{t}{\tau_0^{IH}} - Q\left(\frac{t}{\tau_0^{IH}}\right)^{3/s}\right] \tag{4}$$

The first term (t/τ_0^{IH}) represents the emission of Tb^{3+} ions without ET processes, Q is an ET energy transfer parameter and *s* determines the nature of the involved electric multipole interaction (s = 6, 8, 10 corresponds to the electric dipole-dipole, dipole-quadrupole, and quadrupole-quadrupole interactions, respectively). $Q = \Gamma\left(1-\frac{3}{s}\right)\frac{N_t}{N_0}$, where Γ is the Gamma function, N_t is the number of acceptors per unit volume, N_0^{-1} is the volume of donor's sphere of influence and τ_0^{IH} is intrinsic lifetime.

Fig. 11 shows the plot of $ln\left[-ln\left(\frac{I(t)}{I_0}\right)-\frac{t}{\tau_0^{IH}}\right]$ as a function of $ln\left(\frac{t}{\tau_0^{IH}}\right)^3$, which from Eq. (4) should yield a straight line with a slope of $1/s$. From these fits, the average value of $s = 6.2 \pm 0.7$ was obtained, close to 6 as expected for a dipole-dipole interaction as observed in most Tb^{3+} doped glasses [43,44,46,49]. Using s = 6 we have $Q = \sqrt{\pi}\frac{N_t}{N_0}$, resulting in $N_0 = (1.23 \pm 0.06) \times 10^{20}$ ions.cm^{-3}. In this paper N_t represents the Tb^{3+} ion concentration and the N_t/N_0 ratio indicates the number of acceptors in the donor's sphere of influence. Since $N_0 = 3/(4\pi R_0^3)$ and the donor-acceptor ET parameter $C_{DA} = R_0^6/\tau_0$, we obtained $R_0 = (18.0 \pm 0.8)$ Å and $C_{DA} = (4.5 \pm 0.5) \times 10^{-39}$ cm^6/s. These results are similar to the values obtained in Tb^{3+}-doped phosphate glasses [43].

After this detailed analysis of the fluorescence decay, we can quantitatively analyze the link between the ratio I_G/I_B and the CR process (see Table 2 and Fig. 1). The luminescence ratio is given by

$$\left.\frac{I_G}{I_B}\right|_{lum} = \left(\frac{A_{31}+A_{32}}{A_{41}+A_{42}}\right).\left(\frac{N_3}{N_4}\right) \tag{5}$$

where A_{ij} is the radiative decay rate from levels $i \rightarrow j$ (Fig. 4) and N_i is the level i population density. So, from rate equations we obtain:

$$\frac{N_3}{N_4} = \frac{W_{43}}{W_{3T}} = \frac{A_{43} + W_{43}^* + W_{43}^{CR}}{W_{3T}} \tag{6}$$

In Eq.(6) it was assumed that CR is the only process responsible for the concentration dependence of the fluorescence dynamics of the $^5D_3$ level (level 4 in Fig. 1), while W_{43}^* is a concentration independent term, that can be attributed to phonons, OH^-, host impurities, etc.

The concentration dependence of the fluorescence decay is usually fitted by the empirical expression [48].

$$\tau_4^{exp} = \frac{\tau_{40}^{exp}}{1+\left(\frac{N_t}{N_c}\right)^p} \tag{7}$$

where τ_{40}^{exp} represents the zero-concentration limit of τ_4^{exp} and N_c the critical concentration. The parameters N_c and p are usually obtained from the fit of the experimental data. In this paper, we assumed that the total level 4 decay is given by $W_{4T} = (\tau_4^{exp})^{-1} = A_4 + W_{43}^* + W_{43}^{CR}$. Since W_{43}^{CR} is the only contribution to W_{4T} responsible for its concentration dependence, we can infer from Eq.(7) that $W_{43}^{CR} = (A_4 + W_{43}^*)(N_t/N_c)^{p/3}$. It should be noticed that the level 4 fluorescence quantum efficiency can be estimated by $\eta_4 = \tau_4^{exp}.A_4$. Therefore, from Eqs.(4)–(6), we obtained:

$$\frac{I_G}{I_B} = \frac{\eta_3}{1-\beta_{43}}\left[\beta_{43} + \frac{W_{43}^*}{A_4} + \eta_{04}^{-1}.\left(\frac{N_t}{N_c}\right)^p\right] \tag{8}$$

where $\beta_{43} = A_{43}/A_4$ represents the branching ratio of the $^5D_3 \rightarrow {}^5D_4$ transition, η_3 and η_4 are level 3 and 4 quantum efficiencies, respectively, η_{40} represents the zero-concentration limit of η_4 given by $\eta_{04}^{-1} = (A_4 + W_{43}^*)/A_4$.

In the literature of RE^{3+}-doped materials the Judd–Ofelt (JO) method has been applied successfully to determine the radiative lifetime in several important cases [48]. However, we could not obtain reliable JO calculations in our glasses due to the strong overlapping of the UV absorption lines with the broadband associated with the charge transfer in tungstate groups and the glass UV edge. In fact, there are very few detailed and reliable JO analyses in the literature of Tb^{3+} doped materials [50], since at higher energies the $4f \rightarrow 4f$ transitions are superimposed on more intense absorption bands which arise from $4f^n \rightarrow 4f^{n-1}5d$ transitions. However, Yamashita and Ohishi [21] obtained $\beta_{43} \sim 0.05$ for Tb^{3+}-doped borosilicate glasses, which is the largest β_{43} value we found in the literature for Tb^{3+} doped materials. Therefore, in order to fit the experimental points, we assumed $\beta_{43} << 1$, in Eq. (8) to obtain:

$$\eta_3^{-1}.\frac{I_G}{I_B} \sim \beta_{43} + \frac{W_{43}^*}{A_4} + \eta_{04}^{-1}.\left(\frac{N_t}{N_c}\right)^p \tag{9}$$

where $(\beta_{43} + W_{43}^*/A_4) = \left.\frac{I_G}{I_B}\right|_0$ represents the zero-concentration limit of $\frac{I_G}{I_B}$. Fig. 12 shows the concentration dependence of τ_4^{exp} and $\frac{I_G}{I_B}$, fit by Eqs. (7) and (9), respectively. These fits were performed imposing the same N_c and p values for both fitting curves, since our model establishes a link between these data. The curves in Fig. 12 resulted in $N_c = (1.04 \pm 0.07) \times 10^{20}$ ions.cm^{-3}, $p = (1.9 \pm 0.1)$, $\tau_{40}^{exp} = (1.1 \pm 0.1)$ ms and $\left.\frac{I_G}{I_B}\right|_0 = 2.0 \pm 0.4$. These values are in good agreement with $N_0 = (1.2 \pm 0.2) \times 10^{20}$ ions.cm^{-3}, $\tau_0^{IH} = (1.05 \pm 0.07)$ ms, and $s/3 = (2.1 \pm 0.2)$, respectively, that were obtained by the IH analysis (Fig. 10). Since we expect that $\beta_{43} \ll 1$

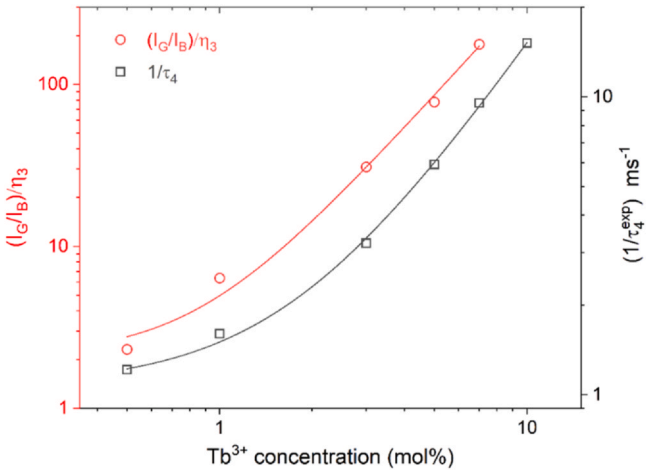

Fig. 12. $1/\tau_4$ (black square) and $(I_G/I_B)\eta_3$ (red circle) Tb concentration dependence fitted by *Eqs. (7) and (9)*, respectively.

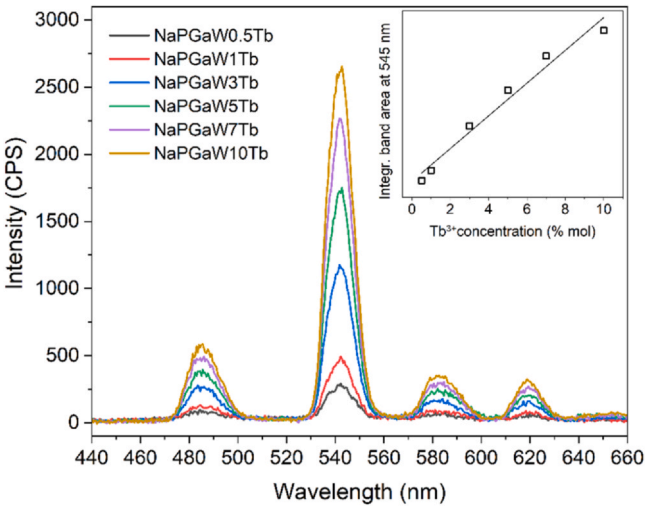

Fig. 13. RL spectra of Tb^{3+} doped gallium tungsten-phosphate glasses. The inset shows the integrated intensity of the $^5D_4 \rightarrow {}^7F_5$ emission line as a function of Tb concentration.

then W_{43}^*/A_4~2.0, η_{04}~$[1 + W_{43}^*/A_4]^{-1}$~ 0.33 and $A_4 \sim \eta_{04}/\tau_{40}^{exp}$ = 300 s^{-1}. These results are very interesting because they allow us to estimate $\eta_4 = A_4\tau_4^{exp}$.

It is interesting to remark that in order to estimate η_3 in Table 2, we assumed that $\tau_3^{rad} \sim \tau_{30}^{exp}$, which appears to be a reasonable assumption due to the large energy gap below $^5D_4$ level. However, the above analyses of $\frac{I_G}{I_B}\Big|_0$ reveals that this assumption is not valid for the $^5D_3$ level since we estimated $\tau_4^{rad} \sim 3.1\ \tau_{40}^{exp}$. The main difference is the energy gaps bellow $^5D_3$ is ~2.6 smaller than $^5D_4$. This affects not only the phonon decay rate (W^{MP}) but also quenching by hydroxyl. Only two OH^- vibrations are required to cover the $^5D_3 \rightarrow {}^5D_4$ decay. For instance, Y. Wang et.a. [52] observed a monotonic increase of I_G/I_B with the absorption coefficient at 3500 cm^{-1} (α_{OH}). This behavior is in agreement with Eq.(9) considering that $W_{43}^* \sim W^{MP} + W^{OH}$, where W^{OH} is supposed to increase linearly with α_{OH}. Also in sol-gel glasses, the I_G/I_B ratio was used to monitor the fluorescence yield of the $^5D_3$ level with the effect of drying agents (to eliminate OH^-) and Al^{3+} co-doping [53]. In fact several papers used I_G/I_B only as a qualitative parameter while this paper allows a quantitative analysis by Eqs.(7–9).

Fig. 13 presents the RL spectra of the NaPGaW:Tb^{3+} glasses. The shape of the characteristic emission peaks is very similar to what was observed for excitation in the UV, as shown in Fig. 8. Nevertheless, the interaction mechanism of X-ray excitation differs substantially from that of UV excitation, which explains the difference of emission quenching observed in the RL spectra. While upon excitation with UV radiation the excitation energy is transferred directly to the Tb^{3+} ions, in the scintillation process, numerous steps occur before rare-earth ion emission [54]. These steps are complex, but they are usually simplified into three consecutive ones. In the first step, *conversion*, the host absorbs the high-energy photon creating electrons and holes. In the second step, known as *migration*, electrons and holes will migrate through the conduction and valence bands, respectively, and a fraction of the electrons and holes recombine at the luminescence centers. This recombination can be radiative, when scintillation occurs, or non-radiative when the energy is lost into heat. This step is called the *relaxation* [2,5]. RL intensity continuously increases for higher Tb concentrations, as shown in the inset of Fig. 13. In the same way, as in the case of the NaPGaW20 glass, the emission of the Tb^{3+} doped samples under UV and X-ray excitation match well with CCD detectors and silicon photomultipliers.

4. Conclusions

Undoped and Tb^{3+} doped gallium tungsten-phosphate glasses have been successfully synthesized by the conventional melt-quenching technique with excellent chemical stability and optical quality. Both, undoped and Tb^{3+}-doped samples present molar density values similar or superior to those of commercially available glass scintillators. The undoped glass presents a broad visible emission (400–750 nm) under UV light and X-ray excitation, ascribed to the radiative decay of STE, characteristic of the tungstate's groups. The doped glasses show intense emissions in the blue-green region and the I_G/I_B depends on the Tb^{3+} concentration. The CIE chromaticity coordinate of the Tb^{3+}-doped NaPGaW glasses were computed. The coordinates tuned from (0.2606, 0.38533) to (0.3261, 0.6042), with the increase of the Tb^{3+} ion content. The chromaticity coordinate of NaPGaW7.0Tb is close to that of the commercial fluorescent powder $MgAl_{11}O_{19}$:0.67Ce^{3+},0.33Tb^{3+} (0.3300, 0.5950), suggesting that NaPGaWTb is a potential candidate for white lighting application. The decay curves of the $^5D_3$ level are found to be non-exponential in nature for all the studied concentrations due to ion-ion energy transfer through cross-relaxation. The lifetime values are in the range 2.6–1.6 ms decreasing for higher Tb concentration. The critical Tb–Tb distance R_c = 18 Å was estimated using the IH-model. It was found that the dipole-dipole interaction mechanism dominates in this glass. This R_c value is similar to values previously reported in other Tb^{3+} doped glasses. A simple model was applied to correlate the I_G/I_B change with the $^5D_3$ fluorescence concentration quenching. This model allows a quantitative estimation of the fluorescence quantum yield of the $^5D_3$ levels without the need of Judd-Ofelt calculations, which are difficult to obtain from Tb^{3+} doped glasses. Despite the presence of the cross-relaxation energy transfer, the optimum concentrations of dopant was determined to be around 7 mol% under UV excitation. From the viewpoint of scintillation, the glasses do not present luminescence quenching (at least up to 10 mol% Tb doping). These results indicate that both, undoped and doped glasses might be a promising alternative to current commercially used glasses as an X-ray scintillator for slow rate events.

Authors contributions

TAL e JFMS contributed equally to this manuscript.

CRediT authorship contribution statement

Thiago A. Lodi: Conceptualization, Methodology, Investigation, Data curation, Writing – original draft preparation. **Jéssica F. M. dos Santos:** Conceptualization, Investigation, Data curation, Formal analysis, Writing – original draft preparation. **Gustavo Galleani:** Conceptualization, Investigation, Writing – reviewing and editing. **Luis G. Jacobsohn:** Data curation, Writing – reviewing and editing. **Tomaz Catunda:** Investigation, Writing – reviewing and editing, Supervision. **Andrea S. S. de Camargo:** Conceptualization, Writing – reviewing and editing, Supervision.

Declaration of Competing Interest

The authors declare that they have no known competing financial interests or personal relationships that could have appeared to influence the work reported in this paper.

Acknowledgments

Authors would like to acknowledge the Brazilian funding agencies FAPESP - Fundação de Amparo à Pesquisa do Estado de São Paulo (Process number 2013/07793-6, CEPID program); CAPES - Coordenação de Aperfeiçoamento de Pessoal de Nível Superior; CNPq - Conselho Nacional de Desenvolvimento Científico e Tecnológico (Universal project 130562/2018-1) and GG acknowledges funding by FAPESP, (grant number 2018/03931-9). L.G. Jacobsohn's contribution was supported by the National Science Foundation under Grant No. 1653016.

REFERENCES

[1] P. Lecoq, A. Gektin, M. Korzhik, Inorganic Scintillators for Detector Systems, second ed., Springer, Berlim, Germany, 2017.
[2] G. Bizarri, Scintillation mechanisms of inorganic materials: from crystal characteristics to scintillation properties, J. Cryst. Growth 312 (2010) 1213–1215, https://doi.org/10.1016/j.jcrysgro.2009.12.063
[3] C. Dujardin, E. Auffray, E. Bourret, P. Dorenbos, P. Lecoq, M. Nikl, A.N. Vasil'ev, A. Yoshikawa, R. Zhu, Needs, trends and advances in inorganic scintillators, IEEE Trans. Nucl. Sci. 65 (2018) 1977–1997, https://doi.org/10.1109/TNS.2018.2840160
[4] M.J. Weber, Inorganic scintillators: today and tomorrow, J. Lumin. 100 (2002) 35–45, https://doi.org/10.1016/S0022-2313(02)00423-4
[5] T. Yanagida, Inorganic scintillating materials and scintillation detectors, Proc. Jpn. Acad. 94 (2018) 75–97, https://doi.org/10.2183/pjab.94.007
[6] T. Yanagida, Study of rare-earth-doped scintillators, Opt. Mater. 35 (2013) 1987–1992, https://doi.org/10.1016/j.optmat.2012.11.002
[7] R.J. Ginther, J.H. Schulman, Glass scintillators, IRE Trans. Nucl. Sci. 5 (1958) 92–95, https://doi.org/10.1109/TNS2.1958.4315633
[8] X. Sun, M. Gu, M. Zhang, S. Huang, Influence of CeO2 on scintillating properties of Tb3+-doped silicate glasses, J. Rare Earths 28 (2010) 340–344, https://doi.org/10.1016/S1002-0721(09)60267-2
[9] J.C. Filho, S.C. Zilio, D.N. Messias, V. Pilla, A.C. Almeida Silva, N.O. Dantas, A.A. Andrade, Effects of aluminum substitution by potassium in the P2O5–Al2O3–Na2O–K2O phosphate glasses, J. Alloy. Compd. 815 (2020) 152359, https://doi.org/10.1016/j.jallcom.2019.152359
[10] I.C. Pinto, G. Galleani, L.G. Jacobsohn, Y. Ledemi, Y. Messaddeq, A.S.S. de Camargo, Fluorophosphate glasses doped with Eu3+ and Dy3+ for X-ray radiography, J. Alloy. Compd. 863 (2021) 158382, https://doi.org/10.1016/j.jallcom.2020.158382
[11] M.W. Kielty, L. Pan, M.A. Dettmann, V. Herrig, U. Akgun, L.G. Jacobsohn, Luminescence of Ce-doped aluminophosphate glasses, J. Mater. Sci. Mater. Electron. 30 (2019) 16774–16780, https://doi.org/10.1007/s10854-019-01301-4
[12] J.C. Knowles, K. Franks, I. Abrahams, Investigation of the solubility and ion release in the glass system K2O-Na2O-CaO-P2O5, Biomaterials 22 (2001) 3091–3096, https://doi.org/10.1016/S0142-9612(01)00057-6
[13] G. Li, C. Zhang, P. Song, P. Zhu, K. Zhu, J. He, Luminescence properties in Tb3+/Yb3+ codoped phosphate glasses for solar cells, J. Alloy. Compd. 662 (2016) 89–93, https://doi.org/10.1016/j.jallcom.2015.12.074
[14] S.M. Salem, Dielectric properties, conductivity, UV–visible and infrared spectroscopy of PbO P2O5 NaF glasses containing WO3, J. Non Cryst. Solids 358 (2012) 1410–1416, https://doi.org/10.1016/j.jnoncrysol.2012.03.020
[15] A. Łapa, M. Cresswell, I. Campbell, P. Jackson, W.H. Goldmann, R. Detsch, A.R. Boccaccini, Gallium- and cerium-doped phosphate glasses with antibacterial properties for medical applications, Adv. Eng. Mater. 22 (2020) 1901577, https://doi.org/10.1002/adem.201901577
[16] M.S. Sadeq, B.O. El-bashir, A.H. Almuqrin, M.I. Sayyed, The tungsten oxide within phosphate glasses to investigate the structural, optical, and shielding properties variations, J. Mater. Sci. Mater. Electron. 32 (2021) 12402–12413, https://doi.org/10.1007/s10854-021-05871-0
[17] A.M. Deliormanlı, Synthesis and characterization of cerium- and gallium-containing borate bioactive glass scaffolds for bone tissue engineering, J. Mater. Sci. Mater. Med. 26 (2015) 67, https://doi.org/10.1007/s10856-014-5368-0
[18] J. Ren, H. Eckert, Intermediate role of gallium in oxidic glasses: Solid state NMR structural studies of the Ga2O3-NaPO3 system, J. Phys. Chem. C. 118 (2014) 15386–15403, https://doi.org/10.1021/jp504023k
[19] N. Wantana, E. Kaewnuam, B. Damdee, S. Kaewjaeng, S. Kothan, H.J. Kim, J. Kaewkhao, Energy transfer based emission analysis of Eu3+doped Gd2O3-CaO-SiO2-B2O3 glasses for laser and X-rays detection material applications, J. Lumin. 194 (2018) 75–81, https://doi.org/10.1016/j.jlumin.2017.10.004
[20] C.C. Lin, W.T. Chen, C.I. Chu, K.W. Huang, C.W. Yeh, B.M. Cheng, R.S. Liu, UV/VUV switch-driven color-reversal effect for Tb-activated phosphors, Light Sci. Appl. 5 (2016), https://doi.org/10.1038/lsa.2016.66 (e16066-e16066).
[21] T. Yamashita, Y. Ohishi, Concentration and temperature effects on the spectroscopic properties of Tb3+ doped borosilicate glasses, J. Appl. Phys. 102 (2007) 123107, https://doi.org/10.1063/1.2821789
[22] Q. Chen, D. Valiev, S. Stepanov, J. Ding, L. Liu, C. Li, H. Lin, Y. Zhou, F. Zeng, Influence of the Tb3+ concentration on the luminescent properties of high silica glass, Opt. Mater. 86 (2018) 606–610, https://doi.org/10.1016/j.optmat.2018.10.008
[23] K. Linganna, V.B. Sreedhar, C.K. Jayasankar, Luminescence properties of Tb3+ ions in zinc fluorophosphate glasses for green laser applications, Mater. Res. Bull. 67 (2015) 196–200, https://doi.org/10.1016/j.materresbull.2015.02.062
[24] G.B. Spector, T. McCollum, A.R. Spowart, Advances in terbium-doped, lithium-loaded scintillator glass development, Nucl. Inst. Methods Phys. Res. A 326 (1993) 526–530, https://doi.org/10.1016/0168-9002(93)90855-C
[25] S. Jia, L. Huang, D. Ma, Z. Tai, S. Zhao, D. Deng, H. Wang, G. Jia, Y. Hua, Q. Yang, S. Xu, Luminescence properties of Tb3+-doped oxyfluoride scintillating glasses, J. Lumin. 152 (2014) 241–243, https://doi.org/10.1016/j.jlumin.2013.12.036
[26] N. Wantana, E. Kaewnuam, Y. Ruangtaweep, D. Valiev, S. Stepanov, K. Yamanoi, H.J. Kim, J. Kaewkhao, Radio, cathodo and photoluminescence investigations of high density WO3-Gd2O3-B2O3 glass doped with Tb3, Radiat. Phys. Chem. 164 (2019) 108350, https://doi.org/10.1016/j.radphyschem.2019.108350
[27] S. Qian, L. Huang, S. Zhao, S. Xu, Luminescent properties of Tb3+doped high density borogermanate scintillating glasses, J. Rare Earths 35 (2017) 787–790, https://doi.org/10.1016/S1002-0721(17)60977-3
[28] X.Y. Sun, Q.M. Yang, P. Gao, H.S. Wu, P. Xie, Luminescence, energy transfer properties of Tb3+/Gd3+-coactivated oxyfluoride borogermanate scintillating glasses, J. Lumin. 165 (2015) 40–45, https://doi.org/10.1016/j.jlumin.2015.04.021
[29] C.W.E. van, E. Delft, Inorganic scintillators in medical imaging, Phys. Med. Biol. 85 (2002) R85–R106, https://doi.org/10.1016/S0168-9002(03)01542-0
[30] Y. Zou, W. Zhang, C. Li, Y. Liu, H. Luo, Construction and test of a single sphere neutron spectrometer based on pairs of 6Li-and 7Li-glass scintillators, Radiat. Meas. 127 (2019) 106148, https://doi.org/10.1016/j.radmeas.2019.106148
[31] D. Manzani, R.G. Fernandes, Y. Messaddeq, S.J.L. Ribeiro, F.C. Cassanjes, G. Poirier, Thermal, structural and optical properties of new tungsten lead-pyrophosphate glasses, Opt. Mater. 33 (2011) 1862–1866, https://doi.org/10.1016/j.optmat.2011.02.041
[32] M. Nalin, G. Poirier, S.J.L. Ribeiro, Y. Messaddeq, L. Cescato, Glasses in the SbPO4-WO3 system, J. Non Cryst. Solids 353 (2007) 1592–1597, https://doi.org/10.1016/j.jnoncrysol.2007.01.031
[33] T. Scheike, H. Segawa, S. Inoue, Y. Wada, Blue luminescence in the WO3-P2O5-ZnO glass system, Opt. Mater. 34 (2012) 1488–1492, https://doi.org/10.1016/j.optmat.2012.03.014
[34] H. Wen, B. Cheng, P.A. Tanner, Optical properties of selected 4d and 5d transition metal ion-doped glasses, RSC Adv. 7 (2017) 26411–26419, https://doi.org/10.1039/C7RA04062H
[35] V.N. Kolobanov, I.A. Kamenskikh, V.V. Mikhailin, I.N. Shpinkov, D.A. Spassky, B.I. Zadneprovsky, L.I. Potkin, G. Zimmerer, Optical and luminescent properties of anisotropic tungstate crystals, Nucl. Instrum. Methods Phys. Res. Sect. A Accel. Spectrom. Detect. Assoc. Equip. 486 (2002) 496–503, https://doi.org/10.1016/S0168-9002(02)00760-X
[36] M.V. Korzhik, V.B. Pavlenko, T.N. Timoschenko, V.A. Katchanov, A.V. Singovskii, A.N. Annenkov, V.A. Ligun, I.M. Solskii, J.P. Peigneux, Spectroscopy and origin of radiation centers and scintillation in PbWO4 single crystals, Phys. Status Solidi Appl. Res. 154 (1996) 779–788, https://doi.org/10.1002/pssa.2211540231
[37] R. Leonelli, J.L. Brebner, Time-resolved spectroscopy of the visible emission band in strontium titanate, Phys. Rev. B 33 (1986) 8649–8656, https://doi.org/10.1103/PhysRevB.33.8649
[38] E. Orhan, F.M. Pontes, C.D. Pinheiro, E. Longo, P.S. Pizani, J.A. Varela, E.R. Leite, T.M. Boschi, A. Beltrán, J. Andrés, Theoretical and experimental study of the relation between photoluminescence and structural disorder in barium and strontium titanate thin films, J. Eur. Ceram. Soc. 25 (2005) 2337–2340, https://doi.org/10.1016/j.jeurceramsoc.2005.03.053
[39] L.S. Cavalcante, M.F.C. Gurgel, A.Z. Simões, E. Longo, J.A. Varela, M.R. Joya, P.S. Pizani, Intense visible photoluminescence in Ba (Zr0.25Ti 0.75)O3 thin films, Appl. Phys. Lett. 90 (2007) 14–17, https://doi.org/10.1063/1.2425013
[40] M. Itoh, T. Katagiri, T. Aoki, M. Fujita, Photo-stimulated luminescence and photo-induced infrared absorption in ZnWO4, Radiat. Meas. 42 (2007) 545–548, https://doi.org/10.1016/j.radmeas.2007.01.049
[41] L. Wang, Y. Ma, H. Jiang, Q. Wang, C. Ren, X. Kong, J. Shi, J. Wang, Luminescence properties of nano and bulk ZnWO4 and their charge transfer transitions, J. Mater. Chem. C 2 (2014) 4651–4658, https://doi.org/10.1039/c4tc00245h
[42] P. Pavan, G. Zanella, R. Zannoni, P. Polato, Radiation damage and annealing of scintillating glasses, Nucl. Inst. Methods Phys. Res. B. 61 (1991) 487–490, https://doi.org/10.1016/0168-583X(91)95326-9

[43] T.O. Sales, R.J. Amjad, C. Jacinto, M.R. Dousti, Concentration dependent luminescence and cross-relaxation energy transfers in Tb3+ doped fluoroborate glasses, J. Lumin. 205 (2019) 282–286, https://doi.org/10.1016/j.jlumin.2018.09.031
[44] A.D. Sontakke, K. Biswas, K. Annapurna, Concentration-dependent luminescence of Tb3+ ions in high calcium aluminosilicate glasses, J. Lumin. 129 (2009) 1347–1355, https://doi.org/10.1016/j.jlumin.2009.06.027
[45] J.F.M. Dos Santos, I.A.A. Terra, N.G.C. Astrath, F.B. Guimarães, M.L. Baesso, L.A.O. Nunes, T. Catunda, Mechanisms of optical losses in the 5D4 and 5D3 levels in Tb3+ doped low silica calcium aluminosilicate glasses, J. Appl. Phys. 117 (2015) 053102, https://doi.org/10.1063/1.4906781
[46] C.R. Kesavulu, A.C. Almeida Silva, M.R. Dousti, N.O. Dantas, A.S.S. De Camargo, T. Catunda, Concentration effect on the spectroscopic behavior of Tb3+ ions in zinc phosphate glasses, J. Lumin. 165 (2015) 77–84, https://doi.org/10.1016/j.jlumin.2015.04.012
[47] D. De Graaf, S.J. Stelwagen, H.T. Hintzen, G. De With, Tb3+ luminescence as a tool to study clustering of lanthanide ions in oxynitride glasses, J. Non Cryst. Solids 325 (2003) 29–33, https://doi.org/10.1016/S0022-3093(03)00324-7
[48] W.J. Miniscalco, Optical and electronic properties of rare earth ions in glasses, Rare-Earth-Doped Fiber Lasers and Amplifiers, second ed., CRC Press, New York, 2001, p. 798, https://doi.org/10.1201/9780203904657
[49] M. Inokuti, F. Hirayama, Influence of energy transfer by the exchange mechanism on donor luminescence, J. Chem. Phys. 43 (1965) 1978–1989, https://doi.org/10.1063/1.1697063
[50] J.F.M. dos Santos, V.S. Zanuto, A.C.C. Soares, E. Savi, L.A.O. Nunes, M.L. Baesso, T. Catunda, Evaluating the link between blue-green luminescence and cross-relaxation processes in Tb3+-doped glasses, J. Lumin. 240 (2021) 118430, https://doi.org/10.1016/j.jlumin.2021.118430
[51] K. Linganna, S. Ju, C. Basavapoornima, V. Venkatramu, C.K. Jayasankar, Luminescence and decay characteristics of Tb3+-doped fluorophosphate glasses, J. Asian Ceram. Soc. 6 (2018) 82–87, https://doi.org/10.1080/21870764.2018.1442674
[52] Y. Wang, S. Liu, J. Mao, X. Li, L. Li, H. Zeng, G. Chen, Study on mechanism controlling 5D3/5D4emissions of Tb3+ in glasses, J. Lumin. 185 (2017) 241–246, https://doi.org/10.1016/j.jlumin.2017.01.028
[53] A.J. Silversmith, N.T.T. Nguyen, D.L. Campbell, D.M. Boye, C.P. Ortiz, K.R. Hoffman, Fluorescence yield in rare-earth-doped sol-gel silicate glasses, J. Lumin. 129 (2009) 1501–1504, https://doi.org/10.1016/j.jlumin.2009.03.026
[54] X.Y. Sun, S.M. Huang, Tb3+-activated SiO2-Al2O3-CaO-CaF2 oxyfluoride scintillating glass ceramics, Nucl. Instrum. Methods Phys. Res. Sect. A Accel. Spectrom. Detect. Assoc. Equip. 621 (2010) 322–325, https://doi.org/10.1016/j.nima.2010.04.032